

Triboelectric–Thermoelectric Hybrid Nanogenerator for Harvesting Energy from Ambient Environments

Ying Wu, Shuangyang Kuang, Huayang Li, Hailu Wang, Rusen Yang, Yuan Zhai,* Guang Zhu,* and Zhong Lin Wang*

Recently developed triboelectric nanogenerators (TENG) with advantages of a low fabrication cost, high output voltage, and high energy conversion efficiency have shown potential applications in harvesting ambient environment energy. However, the heat energy produced and wasted during the triboelectric energy generation process limits the output of TENG. One approach is to design TENG based on a noncontact mode to minimize the energy loss. The other approach is to scavenge the lost energy with a supplementary nanogenerator. In this work, triboelectric–thermoelectric hybrid nanogenerator (TTENG) is fabricated to harvest the energy from ambient environment and the thermal energy from the temperature difference induced by r-TENG friction. At a rotation rate of 500 rpm, r-TENG can produce a constant open-circuit voltage (V_{oc}) of 200 V and a short-circuit current (I_{sc}) of 0.06 mA. The thermoelectric nanogenerator (TMENG) with a size of 16 cm² can produce a V_{oc} of 0.2 V and an I_{sc} of 20 mA. The experimental results show that the TTENG is a promising method to harvest the ambient mechanical energy.

with different converting mechanism have been reported, such as electromagnetic generators,^[4,5] piezoelectric generators,^[6–8] electrostatic generators,^[9–11] and triboelectric nanogenerators.^[12–14] Triboelectric nanogenerators have shown advantages of a low fabrication cost, high output voltage, and high energy conversion efficiency. However, heat energy is produced and wasted during the triboelectric energy generation process, which limits the output of triboelectric nanogenerators (TENG).^[15] On the one hand, noncontact approaches have been used to minimize the energy loss of TENG. On the other hand, it is possible to scavenge the lost energy to improve the output performance of TENG.^[16,17] Although pyroelectric nanogenerators harvesting thermal energy from the friction-induced temperature fluctuation have been reported, different thermal harvesting efforts are

still needed to enhance the total efficiency of the generators that integrates the energy harvesters and the energy storage devices.^[18–20]

Here, we present triboelectric–thermoelectric hybrid nanogenerator (TTENG), which can harvest mechanical and thermal energy. The TTENG is composed of a 2D rotary TENG


1. Introduction

With an increasing energy demands, more and more new generators have been developed to harvest ambient environment energy,^[1–3] which show potential applications in daily life, industrial plants, agriculture, and military. Many generators

Dr. Y. Wu, Dr. Y. Zhai
College of Electrical and Information Engineering
Chongqing University of Science & Technology
Chongqing 401331, China
E-mail: cqzhy@cqust.edu.cn

Dr. S. Kuang, Dr. H. Li, H. Wang, Prof. G. Zhu, Prof. Z. L. Wang
CAS center for Excellent in Nanoscience
Beijing Key Laboratory of Micro-nano Energy and Sensor
Beijing Institute of Nanoenergy and Nanosystems
Chinese Academy of Sciences
Beijing 100083, China
E-mail: zhuguang@binn.cas.cn; zhong.wang@mse.gatech.edu

Dr. S. Kuang, Dr. H. Li, H. Wang, Prof. Z. L. Wang
School of Nanoscience and Technology
University of Chinese Academy of Science
Beijing 100049, China

 The ORCID identification number(s) for the author(s) of this article can be found under <https://doi.org/10.1002/admt.201800166>.

Prof. R. Yang
School of Advanced Materials and Nanotechnology
Xidian University
Xian 710126, China

Prof. G. Zhu
Department of Mechanical, Material and Manufacturing Engineering
University of Nottingham Ningbo China
Ningbo 315100, China

Prof. G. Zhu
New Materials Institute
University of Nottingham Ningbo China
Ningbo 315100, China

Prof. Z. L. Wang
School of Materials Science and Engineering
Georgia Institute of Technology
Atlanta, GA 30332-0245, USA

DOI: 10.1002/admt.201800166

(r-TENG) and thermoelectric nanogenerator (TMENG) based on Seebeck effect. By harvesting the majority of mechanical energy during the rotating motion, the r-TENG can produce a constant open-circuit voltage (V_{oc}) of 2.5 V and a short-circuit current (I_{sc}) of 0.4 mA at a rotation rate of 500 rpm through the transformer. The TMENG with a size of 16 cm² can harvest thermal energy generated by the r-TENG and produce a V_{oc} of 0.2 V and an I_{sc} of 20 mA. The TTENG can produce a V_{oc} of 4.6 V and an I_{sc} of 0.4 mA at a rotation rate of 500 rpm when the TENG and the TMENG are in a serial connection. The TTENG has been demonstrated to charge a capacitor of large capacitance and as a power source for a temperature detection module. With these outstanding performances, the TTENG is proven to be a promising method to harvest ambient mechanical energy.

2. Results and Discussion

2.1. Structural Design and Working Principle of the TTENG

The presented hybrid generator has a multilayered structure, which consists of two parts, a rotator and a stator, as sketched in **Figure 1a**. The rotator is composed of three layers: a rigid substrate layer made of acrylic, a layer of sponge and a positive electrification layer made of nylon. The rotator with a diameter of 8 cm is a collection of radially arrayed sectors separated by equal-degree intervals.

The stator has a vertically stacked structure consisting of three layers. First, a layer of Cu was deposited onto an acrylic substrate as two complementary electrodes with the same configuration as the positive electrification layer. Then, a layer of polytetrafluoroethylene (PTFE) was spread out on the Cu surface. The TMENG was inserted between the electrodes and the substrate. The upper surface of the TMENG is completely in contacts with the electrodes plane, which is helpful to harvest the thermal energy produced by the r-TENG and thus improve the energy conversion efficiency.

The TMENG has five layers, as shown in **Figure 1a**. The first and the last layer are insulators that transmit temperature. The second and the fourth layers are conductors. The third layer

is composed of alternately connected Bi₂Te₃-based P-type and N-type semiconductors.

2.2. Electrical Characterizations

The operation of the r-TENG sensor relies on a relative rotation between the rotator and the stator, in which a unique coupling between triboelectrification and electrostatic induction gives rise to an alternating flow of electrons between electrodes. At the initial state, the rotator is just in contacts with the stator, leading to a charge transfer on the contact surface. A negative charge is produced on the PTFE surface, and a positive charge is produced on the conductive tape.

Under the open-circuit condition, electrons cannot transfer between electrodes. The open-circuit voltage can be defined as the electric potential difference between the two electrodes, namely, $V_{oc} = U_A - U_B$. State I in **Figure 1b** represents the maximum V_{oc} , which corresponds to the maximum potential on electrode A and the minimum potential on electrode B. When the rotator begins to run, V_{oc} diminishes and reaches zero once the rotator reaches the midpoint (state II in **Figure 1b**). As the rotator continues to move, the potential difference increases reversely. When it reaches the terminal point, the reverse potential difference reaches its maximum (state III in **Figure 1b**). Further rotation beyond the final state causes the V_{oc} to change periodically because of the periodic structure (state IV in **Figure 1b**).

The operation of the TMENG relies on the Seebeck effect that refers to the phenomenon of the potential difference generated by the temperature difference. The temperature difference between TMENG's upper end and lower end is zero before the rotator contacts the stator. When the rotator contacts the stator and begins to rotate, the heat energy produced by friction is transferred to the upper end of the TMENG (**Figure 1b**). As a result, electricity is generated due to the Seebeck effect.

The potential difference can be calculated from the following equation^[21]

$$V = \int_{T_1}^{T_2} (S_B(T) - S_A(T)) dT \quad (1)$$

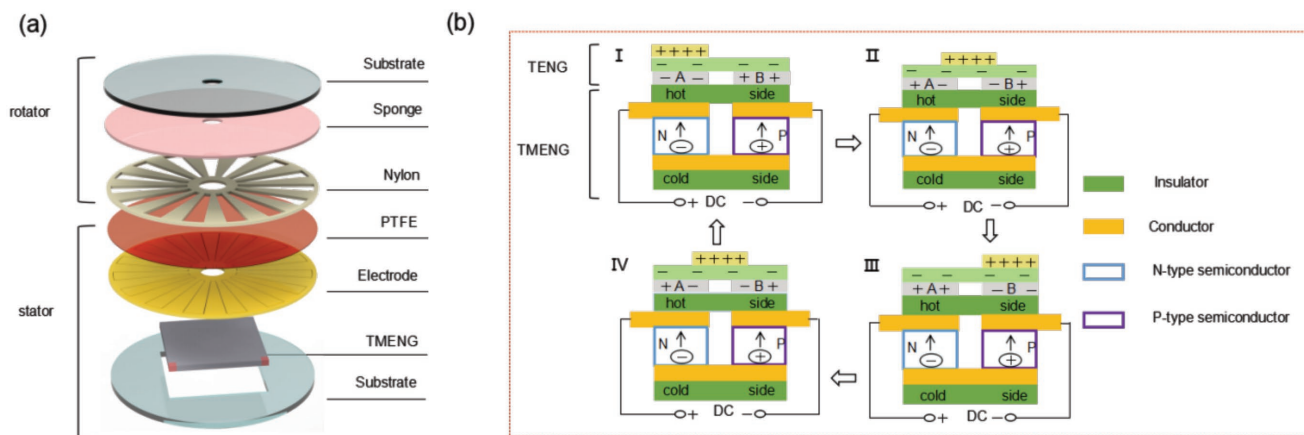


Figure 1. Overall structure and working principle of the TTENG. a) Schematic illustration of the TTENG. b) Detailed schematics of operating principle of the hybrid cell, which include four parts, one initial state (I), two intermediate states (II, IV), and one final state (III).

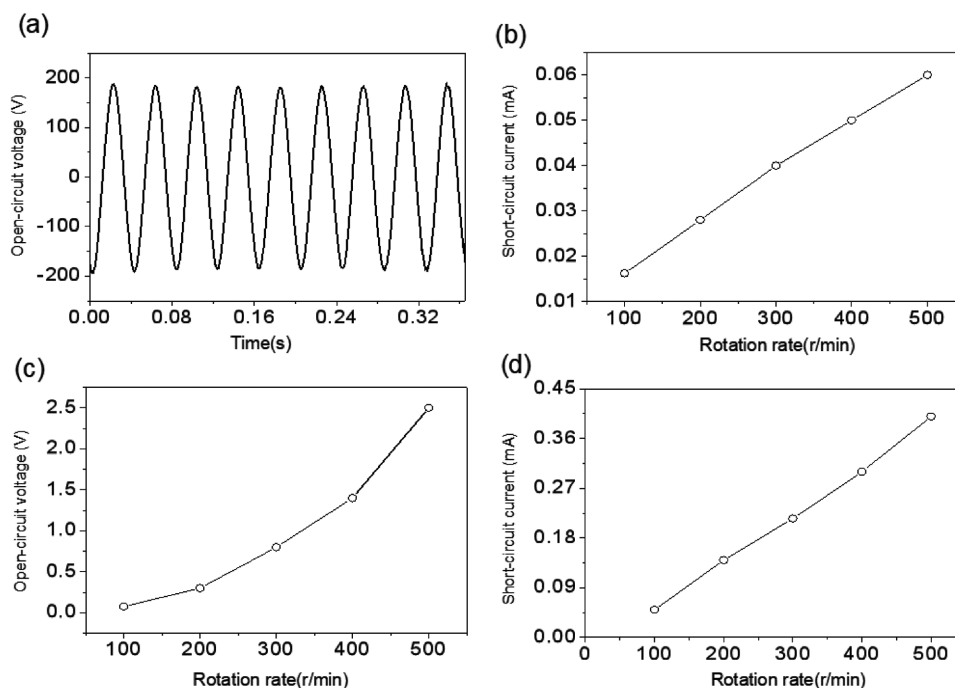


Figure 2. The output of the r-TENG. a) The output voltage of the r-TENG. b) The peak current of the r-TENG. c) The peak voltage of the r-TENG connected to a transformer. d) The peak current of the r-TENG connected to a transformer.

S_A and S_B are the corresponding Seebeck coefficients, and the equation above can be converted into another form once S_A and S_B do not change with the temperature.

$$V = (S_A - S_B)(T_2 - T_1) \quad (2)$$

The performance of the r-TENG was measured while the rotator was sliding on the stator periodically. As shown in **Figure 2a**, the open-circuit voltage oscillated with a peak-to-peak value of 200 V at a rotation rate of 500 rpm. The open-circuit voltage does not change with the increasing of rotation rate because the voltage is only dependent on the position of the rotator, which has been reported previously.^[22] The short circuit current was measured to be an AC output. As shown in **Figure 2b**, the short circuit current I_{sc} increases with the increase of rotation rate and can reach 60 μ A at a rotation rate of 500 rpm. Typically, the r-TENG is connected to a transformer to provide power for the load. As shown in **Figure 2c,d**, with the increase of rotation rate, the open-circuit voltage and the short-circuit current both increase. At the rotation rate of 500 rpm, I_{sc} and V_{oc} can reach 400 μ A and 2.5 V, respectively. The reason for the voltage increase is that the inductive reactance is generated, and the total impedance increased when the transformer is connected. The current changed with the variation of the rotation rate. Therefore, the transformed voltage increased as the rotation rate increased. The detailed reason was elaborated by Zhu.^[22]

As shown in **Figure 3a,b**, the corresponding open-circuit voltage and short-circuit current of the TMENG were measured at different temperature differences. There is a linear relationship between I_{sc} and temperature difference, as well as between V_{oc} and temperature. When the temperature

difference reaches ≈ 33 $^{\circ}$ C, V_{oc} can reach ≈ 250 mV and I_{sc} can reach 30 mA. To observe the output signal resulting from the friction-induced temperature fluctuation during the triboelectric process, the performance of TMENG was measured in all processes of the rotational motion. To compare with r-TENG, the relationship between the corresponding stable output signal of TMENG and the rotation rate was measured. As shown in **Figure 3c**, with the increase of rotation rate, the short-circuit current also increased. The increasing rate of the short-circuit current is faster with the increase of rotation rate. When the rotation rate was set to 500 rpm, the short-circuit current of TMENG was able to reach 20 mA, which is much larger than that of the r-TENG. It can also be observed that the output voltage of TMENG was low and only reached 200 mV when the rotation rate was set to 500 rpm (**Figure 3d**).

The inset of **Figure 3c** shows the short-circuit current of the thermoelectric generator. At first, the output short-circuit current was low because the temperature difference between the lower and upper ends of TMENG was constant and low. When the rotator started to rotate, the temperature of TMENG's upper side rose rapidly. Then, the temperature difference between the lower and upper sides of TMENG reached its maximum, resulting in the instant increase of I_{sc} to its maximum of 12 mA. As time went by, a small amount of heat energy was transferred from the upper end to the lower end. Consequently, I_{sc} decreased and eventually stabilized at 7 mA at a constant rotation rate of 200 rpm. It can also be observed from the curve that the output short-circuit current did not show any decay for a long time after reaching its steady state, which effectively proved the reliability of the TMENG for practical applications.

To enhance the thermoelectric current, two TMENGs were connected in parallel, as shown in **Figure 3e,f**. The output

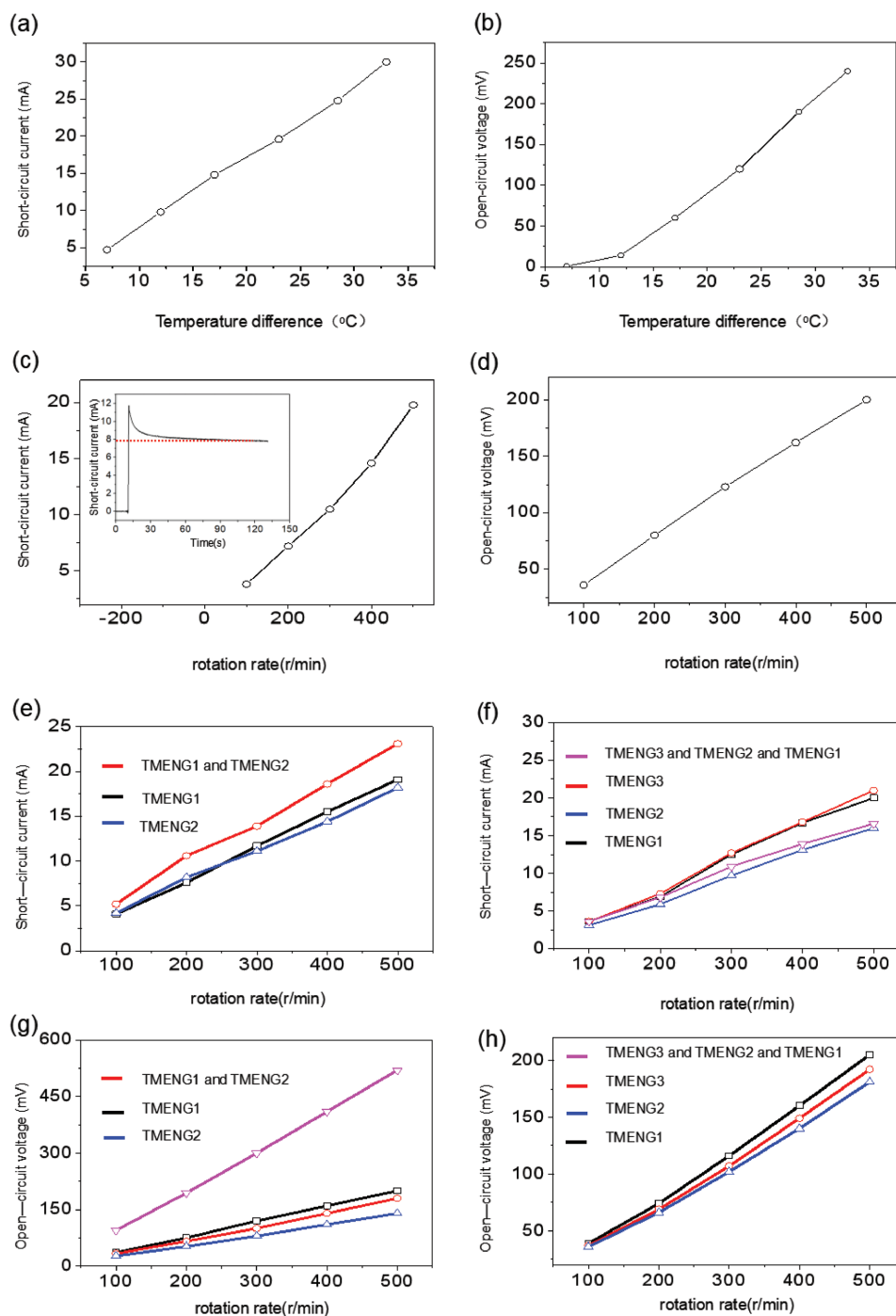


Figure 3. The output of the TMENG. a) The relationship between the current and the temperature difference of one TMENG. b) The relationship between the voltage and the temperature difference of one TMENG. c) The relationship between the current and the rotation rate of one TMENG. d) The relationship between the voltage and the rotation rate of one TMENG. e) The relationship between the current and the rotation rate of two TMENGs in a parallel connection. f) The relationship between the current and the rotation rate of two TMENGs in a serial connection. g) The relationship between the voltage and the rotation rate of three TMENGs in a parallel connection. h) The relationship between the voltage and the rotation rate of three TMENGs in a serial connection.

short-circuit current of the two TMENGs connected in parallel is greater than that of the single output, but lower than the sum of the single output current because the performance of the two TMENGs is not the same. The output current of a

single TMENG is different from that of the TMENG when connected in parallel. Therefore, part of the electronics will flow from one TMENG with a high output current to the other with a low output current, which eventually leads to the fact that

the short-circuit current of TMENGs in a parallel connection is not a linear superposition of the two separate short-circuit currents.

To enhance the open-circuit thermoelectric voltage, three TMENGs were connected in serial. As shown in Figure 3g, the current output of three TMENGs in serial can reach approximately 16 mA at the rotation rate of 500 rpm, because the current output is limited by the minimum current of these three devices. As shown in Figure 3h, the voltage output of the TMENGs connected in serial is a sum of the voltage outputs of the three individual devices and reaches more than 500 mV at the rotation rate of 500 rpm.

2.3. Application

A temperature detection system was successfully driven by the TMENG, demonstrating its application performance. A capacitor with a capacity of 0.5 F was used to store the electricity generated by the TMENG. The charge voltage curve at a rotation rate of 800 rpm is shown in Figure 4a. From the voltage curve, it can be observed that the voltage can reach 0.3 V instantaneously and gradually stabilizes at 1 V in 8 s. The temperature detection system can be powered by ten capacitors connected in parallel. As shown in the Figure 4b,c, the real-time temperature can be detected and sent to the display module, which demonstrates the TMENG's predominant application in a self-powered temperature monitor.

Furthermore, the output performance of TTENG was measured. To get the maximum output voltage, the r-TENG and the TMENG are in a serial connection, as shown in Figure 5a. The corresponding short-circuit was shown in Figure 5b. The output of the TTENG was utilized to power up the light emitting diode (LED) first. When powered by the TTENG, the LED showed a strong illumination intensity, as shown in the red areas in Figure 5b. When the LED was only powered by r-TENG, the LED dimmed gradually and luminance was hardly observed, as shown in the blue areas in Figure 5b.

The peak power densities were measured with different load resistances at the rotation rate of 500 rpm. As the load resistance increased, the power densities for TMENG and TENG were enhanced first and then dropped. The maximum peak power density for TMENG was $\approx 10.5 \text{ W m}^{-2}$ (Figure 5c) at a corresponding load of 6Ω . The output power P can be calculated from the following equation

$$P = UI \quad (3)$$

Where U and I are the load voltage and current, respectively. At the rotation rate of 500 rpm, the maximum output power of TMENG can reach 16.59 mW (the corresponding voltage is 0.395 V, current is 42 mA), and the maximum output power of r-TENG can reach about 4.32 mW (corresponding voltage is 120 V, current is 0.036 mA). It can be concluded that the TMENG can effectively harvest the thermal energy produced by the r-TENG.

As a demonstration for the charging ability of the TTENG, a 22 μF capacitor was charged when the TMENG and the r-TENG were in a serial connection (Figure 5e), and the corresponding charging result is shown in Figure 5f (the red curve). The result of the capacitor solely charged by the r-TENG is shown by the blue curve in Figure 5f. It could be observed that during the same charging time ($\approx 10 \text{ s}$), the charging voltage for r-TENG and TTENG could reach ≈ 1.35 and 1.85 V, respectively. The charging power could be derived from the following equations

$$W = CU^2/2 \quad (4)$$

$$P = W/T \quad (5)$$

where C is the capacitance of the charging capacitor, U is the voltage of the charging capacitor, W is the charging energy of the charging capacitor, P is the power of the charging capacitor, and T is the charging time. From the equations above, the charge efficiency of TTENG is calculated to increase by 87% compared to r-TENG.

3. Conclusions

In summary, we have presented a TTENG composed of r-TENG and TMENG to effectively harvest the ambient mechanical energy. The output power of TTENG was improved greatly because the TMENG could harvest the heat energy created by the friction motion of r-TENG. For the r-TENG, the output power density was able to reach 0.47 mW cm^{-2} at a rotation rate of 500rpm. The open-circuit voltage and the short-circuit current of TMENG were roughly proportional to the temperature difference. The open-circuit voltage and the short-circuit current increased with the rotation speed. These experimental results showed that the output of TMENG was mainly affected

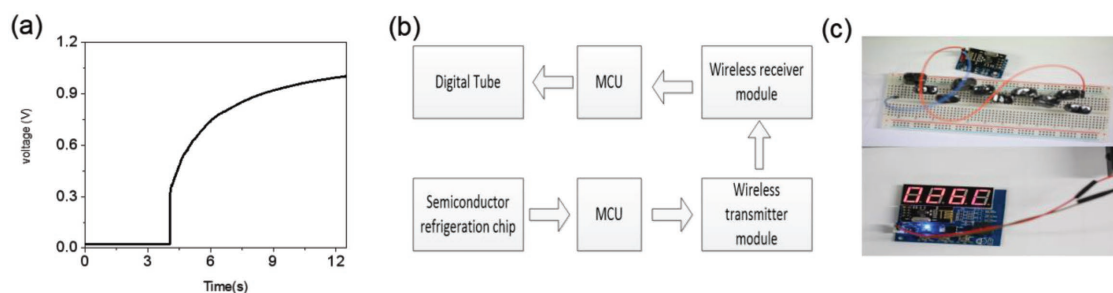


Figure 4. Output performance of a TMENG. a) The voltage curve of a supercapacitor (0.5 F) charged by a TMENG. b) The flow chart of a temperature detection system powered by a TMENG. c) The real display of the temperature detection system powered by a TMENG.

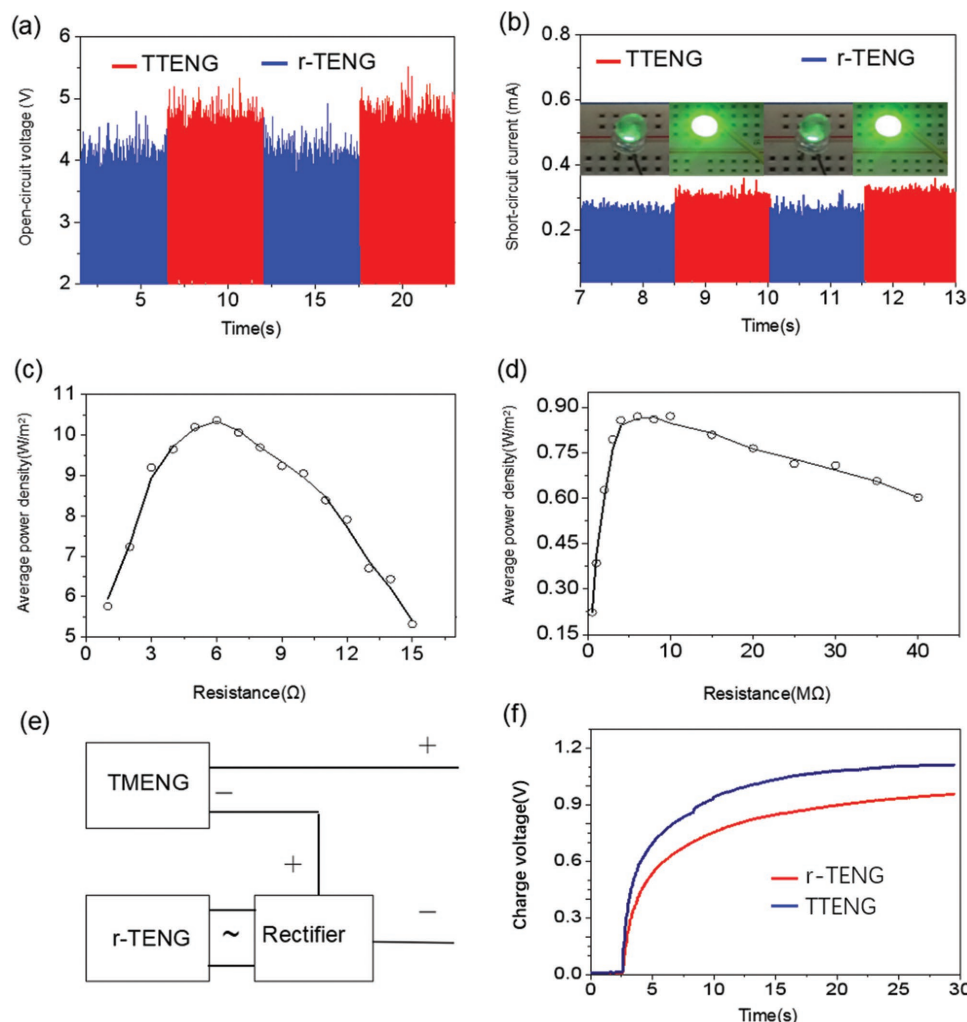


Figure 5. Output performance of the TTENG. a) The voltage of r-TENG and TTENG. b) The current of r-TENG and TTENG. c) The relationship between the instantaneous power density and the resistance of the external load for TMENG. d) The relationship between the instantaneous power density and the resistance of external load for r-TENG. e) The circuit used to integrate the r-TENG and the TMENG. f) The charge voltage curve of r-TENG and TTENG.

by the temperature difference. Under the short-circuit condition, a rising curve of the current was observed at a rotation rate of 500 rpm. The output signal of the TMENGs in serial and parallel modes was measured. A high DC output with a power density of 10.5 W m^{-2} was achieved at a rotation rate of 500 rpm, and a temperature detection system was successfully driven. Furthermore, it was demonstrated that the TTENG's output was able to charge a capacitor, and the charging rate was about three times of the charging rate of a r-TENG. These outstanding performances of TTENGs demonstrate their potential application to harvest ambient mechanical energy.

4. Experimental Section

Fabrication of the TTENG: Rotator: (1) A laser cutter was used to cut a disc-shaped acrylic substrate with patterns that consist of radially arrayed sectors. The rotator has a diameter of 8 cm and a thickness of 1 cm. (2) A through-hole that has a D-profile was drilled at the center

of the rotator. (3) A layer of sponge (1 cm) and then a layer of nylon (0.01 mm) were pasted on the rotator in sequence. Stator: (1) The laser cutter was used to cut a square-shaped acrylic sheet as a substrate with a dimension of 13 cm by 13 cm by 4 mm. (2) Four through-holes were drilled on the edge of the substrate, with which the substrate can be fixed on the experiment platform. (3) The laser cutter was used to cut a square-shaped through-hole at the center of a $4 \text{ cm} \times 4 \text{ cm}$ substrate; (4) The laser cutter was used to create trenches on top of the substrate, and these trenches define the patterns of the two sets of complementary radially arrayed electrodes. (5) The TMENG was embedded into the through-holes, and two lead wires were connected to the TMENG. (6) An electron-beam evaporator was used to deposit a layer of Cu (200 nm) on the substrate. (7) Two lead wires were connected to the Cu electrodes. (8) A layer of PTFE (0.07 mm) was pasted onto the electrode layer.

Setups of the Electrical Measurement: (1) A rotary motor was mounted in an inverted way on a 3D linear positioner. (2) The rotator was fixed on the D-profile shaft of the rotary motor. (3) The linear positioner was used to adjust the height of the rotator so that the rotator and the stator were in firm contact. (4) The position of the linear positioner was adjusted so that the rotator and the stator were aligned in a coaxial alignment. (5) The thermometer was used to record the temperature difference. (6) A Keithley 6514 system electrometer was used to measure voltages and currents.

Acknowledgements

The research was supported by National Key R & D Project from Ministry of Science and Technology, China (Grant No. 2016YFA0202701 & 2016YFA0202703). This research was funded by National Science Foundation of China (Grant No. 51572030). This research was also funded by Chongqing Research Program of Basic Research and Frontier Technology (No. cstc2016jcyjA0236 and cstc2016jcyjA0677) and Research Foundation of Chongqing University of Science & Technology (No. ck2017zkzd005).

Conflict of Interest

The authors declare no conflict of interest.

Keywords

ambient environment harvester, hybrid nanogenerator, thermal energy harvester, thermoelectric nanogenerator, triboelectric nanogenerator

Received: May 18, 2018

Revised: July 2, 2018

Published online:

-
- [1] Y. K. Tan, S. K. Panda, *IEEE Trans. Ind. Electron.* **2011**, *58*, 4424.
[2] K. Ma, Y. Zheng, S. Li, K. Swaminathan, X. Li, Y. Liu, J. Sampson, Y. Xie, V. Narayanan, *High Performance Computer Architecture (HPCA), 2015 IEEE 21st International Symposium on.*, IEEE, Burlingame, February **2015**.
[3] V. Marian, B. Allard, C. Voltaire, J. Verdier, *IEEE Trans. Power Electron.* **2012**, *27*, 4481.
[4] M. Duffy, D. Carroll, *Proceeding of IEEE 35th Annual Power Electronics Specialists Conference*, Aachen, June **2004**.
[5] F. R. Fan, W. Tang, Y. Yao, J. Luo, C. Zhang, Z. L. Wang, *Nanotechnology* **2014**, *25*, 135402.
[6] C. J. Hu, Y. H. Lin, C. W. Tang, M. Y. Tsai, W. K. Hsu, H. F. Kuo, *Adv. Mater.* **2011**, *23*, 2941.
[7] W. S. Jung, M. J. Lee, M. G. Kang, H. G. Moon, S. J. Yoon, S. H. Baek, C. Y. Kang, *Nano Energy* **2015**, *13*, 174.
[8] H. Y. Li, L. Su, S. Y. Kuang, Y. J. Fan, Y. Wu, Z. L. Wang, G. Zhu, *Nano Research* **2017**, *10*, 785.
[9] N. Gogneau, E. Galopin, L. Travers, *Phys. Status Solidi RRL* **2014**, *8*, 414.
[10] A. C. M. De Queiroz, *Circuits and Systems (ISCAS), 2013 IEEE International Symposium on.*, IEEE, Beijing, May **2013**.
[11] A. C. M. D. Queiroz, *Circuits and Systems (ISCAS), 2016 IEEE International Symposium on.*, IEEE, Montréal, May **2016**.
[12] A. C. M. De Queiroz, *Electrostatic Energy Harvesting Without Active Control Circuits*, IEEE, New York, USA **2014**.
[13] F. R. Fan, Z. Q. Tian, Z. L. Wang, *Nano Energy* **2012**, *1*, 328.
[14] G. Zhu, C. Pan, W. Guo, C. Y. Chen, Y. Zhou, R. Yu, Z. L. Wang, *Nano Lett.* **2012**, *12*, 4960.
[15] Y. Yang, W. Guo, K. C. Pradel, G. Zhu, Y. Zhou, Z. L. Wang, *Nano Lett.* **2012**, *12*, 2833.
[16] K. Zhang, X. Wang, Y. Yang, Z. L. Wang, *ACS Nano* **2015**, *9*, 3521.
[17] Z. L. Wang, J. Chen, L. Lin, *Energy Environ. Sci.* **2015**, *8*, 2250.
[18] Y. Yang, J. H. Jung, B. K. Yun, F. Zhang, K. C. Pradel, *Adv. Mater.* **2012**, *24*, 5357.
[19] Y. Yang, S. Wang, Y. Zhang, Z. L. Wang, *Nano Lett.* **2012**, *12*, 6408.
[20] Y. Zi, L. Lin, J. Wang, S. Wang, J. Chen, X. Fan, P. K. Yang, F. Yi, Z. L. Wang, *Adv. Mater.* **2015**, *27*, 2340.
[21] Z. H. Dughai, *Phys. B: Condens. Matter* **2002**, *322*, 205.
[22] G. Zhu, J. Chen, T. Zhang, Q. Jing, Z. L. Wang, *Nat. Commun.* **2014**, *5*, 3426.